Volume 9, Issue 4, 2019, 4050 - 4059 ISSN 2069-5837
Biointerface Research in Applied Chemistry
www.BiointerfaceResearch.com
https://doi.org/10.33263/BRIAC94.050059
Original Research Article Open Access Journal
Received: 15.07.2019 / Revised: 08.08.2019 / Accepted: 10.08.2019 / Published on-line: 15.08.2019

# Modelling and Controlling of ion transport rate efficiency in Proton exchange membrane (PEMFC), alkaline (AFC), direct methanol (DMFC), phosphoric acid (PAFC), direct forming acid(DFAFC) and direct carbon (DCFC) fuel cells

**Fatemeh Mollaamin [1], Thu Thi Pham [1], Dung My Thi Dang [1], Majid Monajjemi [1, 2, *], Chien Mau Dang [1, *]**
[1]Institute for Nanotechnology (INT), Vietnam National University - Ho Chi Minh City (VNUHCM), Ho Chi Minh City, Vietnam
[2]Department of chemical engineering, Central Tehran Branch, Islamic Azad University, Tehran, Iran
*corresponding author e-mail address: ***Maj. Monajjemi@iauctb.ac.ir; dmchien@vnuhcm.edu.vn***

## ABSTRACT
Ion transport rate of DFAFC, PAFC, AFC, PEMFC, DMFC and SOFC fuel cells have been studied. AFC which uses an aqueous alkaline electrolyte is suitable for temperature below 90 degree and is appropriate for higher current applications, while PEMFC is suitable for lower temperature compared to others. Thermodynamic equations have been investigated for those fuel cells in viewpoint of voltage output data. Effects of operating data including temperature (T), pressure (P), proton exchange membrane water content (λ) , and proton exchange membrane thickness ($d_{mem}$) on the optimal performance of the irreversible fuel cells have been studied. Performance of fuel cells was analyzed by simulating polarization and power curves for a fuel cell operating at various conditions with current densities.
**Keywords:** *Fuel cells, PEMFC Fuel cell, AFC Fuel cell, DMFC Fuel cell, DCFC Fuel cell, PAFC Fuel cell, DFAFC Fuel cell.*

## 1. INTRODUCTION

Generally, the fuel cells convert the chemical energies of a fuel (mostly $H_2$) and an oxidizing agent (usually oxygen in the air ) into electricity through a pair of redox reactions [1]. Although there are several kinds of fuel cells, customarily they all consist of, a cathode, an anode, and an electrolyte which allows ions, frequently positively protons ($H^+$) to move between two sides of the fuel cells [1,2]. Briefly, at the anode via a catalyst material and oxidation reaction, ions are generated through electrolytes which move toward the cathode [3]. Simultaneously, in a reverse direction, electrons flow towards the cathode via an external circuit. At the cathodes, various catalysts can be applied to produce ions, electrons, and oxygen for reacting and forming water or some other products. Fuel cells are categorized based on species of their electrolytes and also by the difference in startup time ranging between around one second for PEMFC [4] to ten minutes for solid oxide fuel cells (SOFC) with maximum efficiency among 45% to 60%. In the fuel cell of a solid acid electrolyte, $H^+$ conducting oxyanion salt (solid acid) consists of a solid supported within the membrane which is saturated with $H_2O$ for any further ions transporting. Anode reaction is: $H_2 \rightarrow 2H^+ + 2e^-$ and Cathode reaction is: $1/2\ O_2 + 2e- + 2H^+ \rightarrow H_2O$ and the overall reaction is: $H_2 + 1/2\ O_2 \rightarrow H_2O$. In viewpoint of mechanism, at the anode, $H_2$ first come into contact with a nickel catalyst and break apart, bonding to the nickel surface forming weak H-Ni bonds consequently the oxidation reaction can be proceed. Each $H_2$ releases its electron, which moves around the external circuit to the cathode which is electrical current. Then the $H^+$ bonds with $H_2O$ on the membrane surface for forming $H_3O^+$ that moves through the membrane to the cathode electrode, leaving the nickel catalyst for the next $H_2$. At the cathode, $O_2$ come into contact with a nickel catalyst on the electrode surface and break apart bonding to the nickel sheet forming weak O-Ni bonds, enabling the reduction reaction to proceed. $O_2$ then leaves the nickel catalyst site, combining with two electrons that move in external circuit and two protons which have moved through the membrane for forming $H_2O$. Increasing the $H_2$ storage is a major section for the transition more and more hydrogen molecules in a fuel cell [4, 5]. Direct methanol fuel cell (DMFC) is a subcategory of PEMFC in which methanol is used as the fuel. The advantages which can be considered are the energy-dense, easiness of transport and reasonably stable liquid at all environmental situations and mean- while its disadvantages is low efficiency( around 10%), so they are targeted especially to portable applications, which power densities are more important than the efficiencies[6]. In contrast to indirect fuel cells, which $CH_3OH$ molecules are reacted to $H_2$ molecules via a steam improving, direct form use a $CH_3OH$ solution for transporting the reactant into the cells; common operating temperature is in the range 55–115 °C, which high temperature is generally pressurized [6,7]. Direct methanol fuel cell, itself is more efficient at top temperature and pressure, but these situations finally creating so many problem in whole of system that the advantage windswept, so atmospheric-pressure forms are yet preferred and applied [7, 8].Due to the $CH_3OH$ "cross-over" phenomena or diffusion via the membrane (without reacting), $CH_3OH$ is unsuitable as a solvent, this decreases the performance of fuel cells considerably, since this phenomenon, directly reacts with air (in cathode), consequently reduction of the cell voltage accomplishes, therefore "cross-over" phenomenon is a main problem in inefficiency of direct methanol fuel cells[9].This matter can be reduced through improving membranes, developing catalyst layers , reclaiming the structures of gas layers and optimizing the design of the electrodes (such as management of carbon dioxide at the anode) in viewpoint of current densities distribution [10]. The DMFC has restricted in the

PT factor (power*time factors) which means they can produce the small quantity of power in a lengthy period of time. Of course those are suitable for large vehicles. The half-reactions of DMFC are; in anode (oxidation); $CH_3OH + H_2O \rightarrow 6H^+ + 6e^- + CO_2$ and in cathode (reduction) the half-reaction is $\frac{3}{2}O_2 + 6H^+ + 6e^- \rightarrow 3H_2O$ ; while the overall reaction is: $CH_3OH + \frac{3}{2}O_2 \rightarrow 2H_2O + CO_2$ , The $CH_3OH$ oxidation over the catalyst layers produce $CO_2$ and $H_2O$ is consumed at the anode and is again produced at the cathode [9, 10]. From each reaction 6-proton is transported through the PEM which usually made of from Nafion [2, 7] (sulfonated tetra-fluoro-ethylene based fluoro-polymer-copolymer). Although platinum (Pt) as a Nano particle might be suitable as a catalyst for both anode and cathode, it is very expensive and during oxidation the number of available sites in Pt will be occupied by CO which produced in oxidation of methanol, consequently the efficiency of the cell will be decrease. An alloy of platinum with suitable percentage of Au, Ru and Cu can be removing this problem. Storage of formic acid materials (HCOOH) are secure, safe, and confident compared to $H_2$ , as it is a non-flammable liquid and also does not cross over the polymer membrane, so its performance can be higher than that of methanol. DFAFC convert HCOOH and O2 into CO2 and H2O to produce energy. The half-reactions of DFAFC are: anode; $HCOOH \rightarrow CO_2 + 2H^+ + 2e^-$ and in cathode; $\frac{1}{2}O_2 + 2H^+ + 2e^- \rightarrow H_2O$ and total reaction is $HCCOH + \frac{1}{2}O_2 \rightarrow CO_2 + H_2O$ [11]. The alkaline fuel cell (*Bacon* fuel cell), is one of the important fuel cells with high performance that NASA has applied, in Apollo-series missions and on the Space Shuttles. The half-reactions of DFAFC are: anode; $H_2 + 2OH^- + \rightarrow 2H_2O + 2e^-$

And in cathode; $O_2 + 2H_2O + 4e^- \rightarrow 4OH^-$ . In AFC, two electrodes are divided through a porous martials filled with an alkaline solvent, such as KOH, NaOH or NH4OH. One of the important advantages of these kind fuel cells is that alkaline solutions can be reacting with $CO_2$ to produce conversion $K_2CO_3$. Environmentally, AFC is suitable to clean out as much of the $CO_2$ due to operate (even in high temperature) on pure oxygen, or at least purified air . Since, $O_2$ reduction reaction (ORR) at the cathode is easier than in acidic cells, AFCs in the systems can be operated up to 90 °C with higher performance than acidic electrolyte, such as PEMFC.

**1.2. PEM fuel cells.**

Obviously fuel cells as an electrochemical instrument are able to convert chemical energies straightly into direct electrical currents (DC) through a sufficient electrolyte. Therefore, it is usually far yields than combustion engines. A fuel cell needs a stable reservoir of fuels and oxidants for to keeping the electrochemical reactions, same as hydrogen and oxygen [4, 6, 8-9]. Although Hydrogen can be used in a mixture with other gasses such as $N_2O$, $N_2$, and $NO_2$, the major fuel cell is electrolysis reversed consist of hydrogen and oxygen for producing electricity with high efficiency. It is notable that electrolyte has major roles which are different types this work is focused on graphene and h-BN electrodes with polymer membrane electrolyte (PEM) in low temperature. In the PEM fuels cell, the electrolytes are thin polymeric membrane including proton permeability. At low temperature around 90◦C the presence of a catalyst such as typically nickel is needed for hydrogen oxidation reaction (HOR) and oxygen reduction reaction (ORR) on anode and cathode electrodes respectively (Scheme.1).

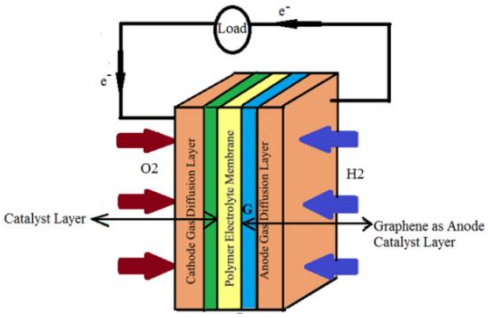


**Scheme 1.** Schematic of a fuel cell.

Cathode and anode gases diffusion layers, generally made of carbon porous including graphene layer for cathode and anode adjacent to catalyst, respectively which are distributed on each side of the polymer membrane. Currently, PEM fuel cell technologies have been combined to the R&D approaches in the automotive sections such as Chrysler, Toyota, Suzuki, Ford, General Motors, Volvo, Hyundai, Nissan and BMW and also as power back-up sources [11-13]. The electrochemical reactions accomplish at the catalyst electrodes on both sides polymer material including oxidation and reduction (equations 1&2). Hydrogen flows into the PEM fuel cell and diffuses through the gases diffusion layers to the catalyst layers, where catalyst particles facilitate fuel oxidation and protons trap onto water molecules to form $H_3O^+$ that move via the membrane from the anode towards cathode. In addition two electrons from above equations (1&2) reach to the cathode electrode over the bipolar plates and over an external circuit. It is notable that this mechanism is known as electro-osmotic drag. On the cathode electrode, oxygen gases diffuse to the catalyst layer and chemically combined with protons and electrons to form water (ORR). Obviously, the electrodes must be selected of porous materials that facilitate water moving to outside and the excess oxygen gases might be help for pushing water out of the cell (scheme 2 & 3)[10-12]. Efficiency, permanence and cost reduction effort are the most important items for PEM fuel cells that cover construction and assembly methods [8]. There are several major items for increasing the life cycle and PEM fuel cells efficiency which are thermal management, water management, new catalysts, and novel material of membranes and also quality of electrodes. Operating conditions and operating strategies play an important role in a fuel cell lifecycle. Bad distribution of fuel cell reactants can appear in the presence of high cell currents, liquid water, fuel impurities, and different flows of fuel due to the sudden changes in the power demand and conditions between cell inlet and outlet [11-13]. In other hand, fuel starvation can cause severe degradation during of gross fuel starvation that cell voltages can become negative (as the anode) and the carbon is consumed given

the lack of fuel, consequently anodic current will be provided by carbon corrosion to form carbon dioxide [12-14]. In addition, oxygen starvation can result in generation of hydrogen in the cathode or oxygen in the anode similarly during oxygen starvation the reaction at the cathode will produce hydrogen. For avoiding these problems the suitable monitoring controlling sensors and indicators are needed [14].

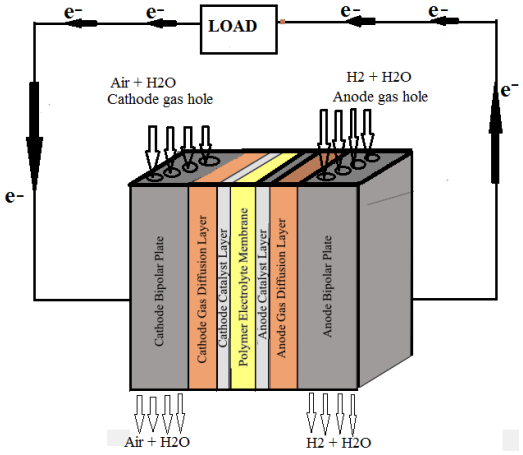


**Scheme 2**. one unit of PEM fuel cell structure.

Several studies have exhibited that improper thermal management is important, higher temperature might be producing the radicals consequently the electrochemical surface area (ECSA) decrease the life time. There are various cooling methods for PEM fuel cells which one important has been investigated among Liquid-cooled air-cooled and evaporative-cooled fuel cells. Water management is essential and most important issues in PEM fuel cell technologies which dependent on adequate membrane hydration and avoidance of water flooding in the catalyst layers. It is important to keep the membrane and the catalyst layer humidified for high proton conductivity. In the presence of $H_2O$, the protons produce $H_3O$+ on the boundaries of the catalyst layer and the membrane which prevent of the proper activity of the protons from the anode catalyst layer to the cathode catalyst layer in aqueous phase. Therefore, tuning humidification of the membranes is also a basic way of cell performance while accumulation of too much water also impacts performance and lifetime. Excess water blockages can instantly lead to reactant starvation and water flooding is an important limiting factor of PEM fuel cell efficiency and life time [15-17]. Flooding appears in both cathode and anode electrodes [13] with three mechanisms as follows; (a) Water generated in the cathode side of the membrane by the electrochemical reaction (ORR), (b) electro-osmotic drag and (c) over-humidified reactant gases. Anode flooding is much longer than the cathode flooding. Although flooding in the cathode is much common compared to anode, flooding on the anode side of the membrane can also have serious consequences on the operation, performance and degradation and due to low fuel flow rates, removing $H_2O$ from anode are much more difficult compared to cathode. Pasaogullari has reported, anode flooding is most probable for happening at low current, low reactant flow rates and low temperatures due to the lower electro-osmotic forces [17].

In other words proton flux is large in the anode electrode; therefore a strong electro-osmotic force pulls the H2O from anode to cathode (due to the low water content). In contrast to the inlet of the anode side, at the exit current density is lower and $H_2$ concentration has decreased, so, the partial pressure of water is high and closer to total anode pressure [18, 19]. Several researchers have assessment of various tactics and technics for water managing. Su et al. [15] & He et al. [20] associated partial pressure straightly to the flooding level and considered it to be a suitable indicator for efficiency. They planned a tool for monitoring the flooding measure in PEM fuel cell with inters digitized flow field. Bosco and coworkers [21] record a USA patent for a simple way which monitors the pressure drop across the flow field to detect flooding in PEM fuel cells. Problem of membrane dehydration is related to drying out in anode which causes a protonic resistance and consequently collapse in cell voltage.

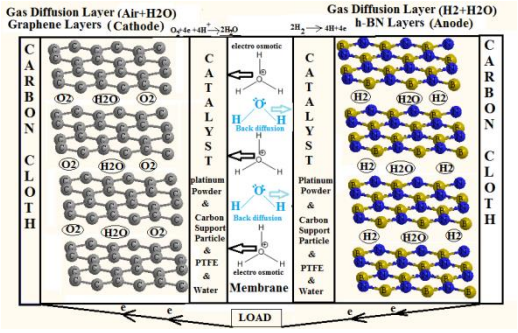


**Scheme 3.** Diffusion through graphene and h-BN.

Therefore in dried situation radicals will produce and increased, to enhanced membrane degradation. Anode dehydration is might be serious both at the inlet of the cell and at the outlet trajectory. In addition due to dehydrating conditions, the membrane leads to lower diffusion. One of the main reasons for dehydration is the strong electro-osmotic forces in the condition of high current densities where water replenishment by reactant humidification or back-diffusion is not quick enough to cope with the lack of water [22].

## 2. MATERIALS AND METHODS

### 2.1. Thermodynamic of fuel cells.

The enthalpy of hydrogen combustion reaction or hydrogen heating amount for one mole of hydrogen can be calculated via $\Delta H = \Delta H_f^0(H2O) - \Delta H_f^0(H2) - \frac{1}{2}\Delta H_f^0(O2) = -286.31\ Kj/mol$

Hydrogen heating amounts are used as a measure of energies input for the fuel cells and this is the maximum value of thermal energy which can be extracted from hydrogen. In addition Gibbs free energy is given by the following equation: ΔG = ΔH - TΔS. which the difference between entropies of products and reactants can be calculated as $\Delta S = \Delta S_f^0(H2O) - \Delta S_f^0(H2) - \frac{1}{2}\Delta S_f^0(O2)$ . The maximum electrical work is:$W_{max} = -n(emf)F$ = -$\Delta G$ where F is Faraday's constant and "emf" is the ideal electro motor force or potential of the cell. Therefore the theoretical hydrogen/oxygen fuel cell potential or maximum voltage of fuel cells is: $emf =$

$E = \frac{-\Delta G}{nF} = \frac{237.342\ J\ mol^{-1}}{2*98486.5\ Coulmb} = 1.231\ Volt$. The thermal efficiency is defined based on amount of useful energy released when a fuel is reacted with an oxidant ($\Delta G$), relative to the change in stored chemical energy ($\Delta H$) therefore the maximum theoretical yields in a fuel cell is $\eta = \frac{\Delta G}{\Delta H} = \frac{237.342}{-286.31} = \%82.9$. Based on Nernst equation a function of temperature and pressure can be applied for any fuel cells as; $emf = E_{(T,P)} = -\left(\frac{\Delta H}{nF} - \frac{T\Delta s}{nF}\right) + \frac{RT}{nF} Ln\left[\frac{P_{H_2} P_{O_2}^{0.5}}{P_{H2O}}\right]$, **(1)** based on this equation, in an open circuit with reactant gases the actual cell potential is decreased (usually less than 1V) and it is called open circuit voltage (OCV). This decreasing of actual cell potential is due to irreversible losses and hydrogen crossover losses which often called polarization, over potential, or over voltage including activation polarization, ohmic polarization and concentration polarization [23]. Activation polarization is associated with sluggish electrode kinetics which happens at both anode and cathode which can be expressed with Tafel equation: $\Delta V_{act} = \frac{RT}{\alpha F} ln \frac{i}{i_0}$ **(2)** where $\alpha$ is the electron transfer coefficient of the reaction at the electrodes and i0 is the exchange current density. The ohmic polarization appears due to resistance against the flow of protons in the electrolyte and also resistance to the flow of electrons through the electrode materials as the equation $\Delta V_{ohm} = i\Omega$ where i is the current flowing through the cell and **Ω** is the total cell resistances consist of electronic, ionic and contact resistance. Concentration polarization is due to loss of potential because of inability of the surrounding material for maintaining the initial concentration of the bulk fluid, thus, a concentration gradient is formed. $\Delta V_{conc} = \frac{RT}{nF} \ln\left[\frac{i_L}{i_L - i}\right]$, That $i_L$ is the limiting current. The actual cell voltage can be written as: $V_{cell} = E(T,P) - (\Delta V_{act} + \Delta V_{conc})_a - (\Delta V_{act} + \Delta V_{conc})_c - \Delta V_{ohm}$ **(3)** by replacing the above equations in this equation the fuel cell polarization curve is: $V_{cell} = E(T,P) - \frac{RT}{\alpha_c F} ln \frac{i}{i_{0,c}} - \frac{RT}{\alpha_a F} ln \frac{i}{i_{0,a}} - \frac{RT}{nF} \ln\left[\frac{i_{L,a}}{i_{L,a} - i}\right] - \frac{RT}{nF} \ln\left[\frac{i_{L,C}}{i_{L,C} - i}\right] - i\Omega$. **(4)** [23, 24]. Due to the activation energy barriers the polarization terms voltage collapse very fast and in the ohmic term polarization voltage falls slower due to the membrane and electrode ohmic resistance. Nernst–Planck equation flux rate of $n_j$ of the species $j$ is given by: $n_j = -D_j \frac{dc_j}{d_x} + C_j \vartheta - \frac{z_j F}{RT} D_j C_j \frac{d\emptyset}{dx}$ , where $D_j$ is the mass diffusivities coefficients and $C_j$ is the concentrations, $\vartheta$ is the solution velocities, $\emptyset$ is the potential gradient. In an electrolyte without concentration gradients, Nernst–Planck equation convert to Ohm's law and current in an electrolyte can be obtained as equation as follows:

$I = nzF = (= -D_j \frac{dc_j}{d_x} + C_j \vartheta - \frac{z_j F}{RT} D_j C_j \frac{d\emptyset}{dx}) Z_j F$[23, 24]. In static electrolyte systems [24], for several classes of fuel cells only diffusions and migrations terms remain. These categories of fuel cells specified via their electrolytes (Table 1). For both Phosphoric acid fuel cells (PAFC) and polymer electrolyte membrane fuel cells (PEMFC), the hydrogen molecules splitting at the anode into hydrogen ions are transport across the electrolyte to the cathode [24-30].

**Table 1.** Fuel Cell Types.

| Fuel cell | Electrolyte Use | Operating temperature | Efficiency Cell | Statues |
|---|---|---|---|---|
| **DFAFC** | Polymer membrane | $<40^0$ | <40% | Commercial Research |
| **AFC** | Aqueous alkaline | $<90^0$ | 60%-70% | Commercial Research |
| **DMFC** | Polymer membrane | 90-120 | 20-30% | Commercial Research |
| **PEMFC** | Polymer membrane | 50-100 (Nafion) 120-200 (PBI) | 25-40% | Commercial Research |
| **Direct carbon fuel cell** | Several different | 700-900 | 70% | Commercial Research |
| **Magnesium air fuel cell** | Salt water | -25-50 | 90% | Commercial Research |
| **Protonic ceramic fuel cell** | $H^+$ conducting ceramic | 700 | | Research |
| **Enzymatic Biofuel Cells** | not denature the enzyme | <40 | | Research |
| **Phosphoric acid fuel cell** | Molten ($H_3PO_4$) | 150-200 | 45% | Commercial Research |

For a PEMFC of static electrolyte with 25cm$^2$ active area, 50µm thickness and $9{\cdot}10^{-7}$cm$^2{\cdot}$s$^{-1}$ diffusion coefficient of H+ ions [25-28], current density obtained for applied potential difference between 0.5-1.0$V$ at 75°C exhibited in Fig.1

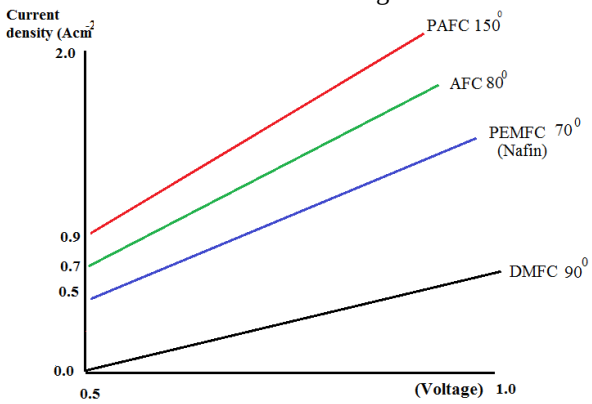


**Figure 1.** Current densities versus potential.

Although PEMFC has a lower current than PAFC, due to its lower operating temperature allowing fast startup and can be applied in automotive power applications. Another advantage of PEMFC is that its electrolyte is a solid material and is less expensive to manufacture than the liquid electrolyte $\eta\,(T,P) = \left(\frac{\Delta H - T\Delta S}{nF}\right) + RTLn(\frac{P_{H_2} P_{O_2}^{0.5}}{P_{H_2O}})$ [25,26]. It is notable that, the maximum electrical energies and the potential differences are achieved when the fuel cells are operating under the thermodynamically reversible condition. Practically, an open circuit potential is considerably lower than the theory due to three main losses which are, first concentration polarization $V_{concen}$ second activation polarization $V_{act}$ , and third ohmic polarization $V_{ohmic}$ . The irreversible voltage loss $V_{irrev}$ is a summation of these three parameters, $V_{irrev} = V_{act} + V_{ohmic} + V_{concen}$ . Based on Butler-Volmer equation, a specific potential is needed for overcoming to the energies barriers which called activation polarization $i = I_c + I_A = i_0 \left[-\exp(-\frac{\alpha_C nF\eta}{RT}\right) + \exp(\frac{\alpha_A nF\eta}{RT})]$ where $I_A$ *and* $I_c$ are anode and cathode current densities, respectively and $i_0$ is the reaction exchange currents densities. Meanwhile $\alpha_A$ and $\alpha_C$ are the charge transfer coefficients at the anode and cathode and $n$ is the number of exchange protons per mole of reactant. Here $\eta$ is the activation over potential term or $\Delta V_{act} = \eta = -\frac{RT}{n\alpha_C F} ln \frac{i}{i_0}$

[26,27]. For a fuel cell operating with a transfer coefficient of 0.45 activation losses versus current density are shown in Fig. 2.

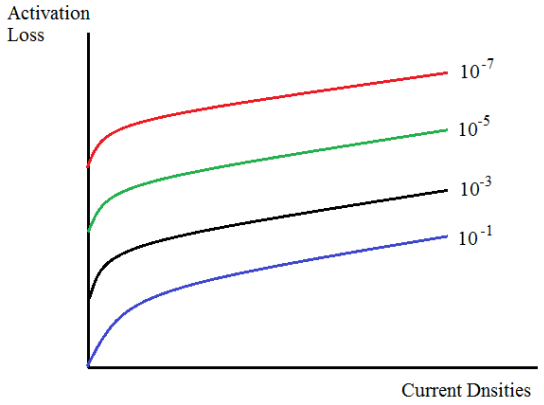


**Figure 2**. Activation loss as a function of current densities.

With an exchange current density of $10^{-3}$Acm$^{-2}$activation losses for different transfer coefficients are shown in Figure3 which indicate that for large exchange current densities, fuel cell has insignificant activation over potential. This is a measure of the system abilities for delivering a net current with significant energies loss. When the transfer's coefficients are low, the activation over potentials is large for any specific current. If the transfer's coefficients are large, the fuel cell will provide large current with small activation over potential. The electrolytes have an intrinsic resistance to prevent the charge flow due to ohmic polarization including $R_{electronic} and R_{ionic}$.Fuel cell resistances can be written as:

$V_{ohmic} = iR_{ohmic} = i(R_{electronic} + R_{ionic})$

$R_{ionic}$ Indicates the ionic resistance and $R_{electronic}$ consist of the total electrical resistance of all components concluding bipolar plates, cell interconnects and all connection path.

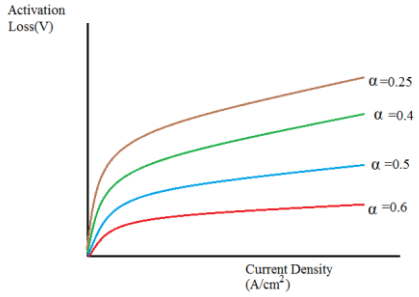


**Figure 3.** Activation loss versus transfer coefficient.

The big amount of ohmic loss appears during the transport of ions through the membrane which depends on membrane water or membrane relative humidity ( $\emptyset_m$ ) parameter as a function of $\lambda = C_0 + C_1\emptyset_m + C_2{\emptyset_m}^2 + C_3{\emptyset_m}^3 + C_4{\emptyset_m}^4 + \ldots$ where $C_n$ are coefficients. It is notable that the resistance of the membrane changes with water because of water uptake results in membrane swelling, which changes the membrane thickness along with its conductivity. The ionic resistance can be written as: $R_{electronic} = \frac{2l_d}{\sigma_d}$ where $l_d$ and $\sigma_d$ are diffusion layers of thickness and electronic conductivities, respectively [25-27]. The concentration over potential is due to the mass transfer of $H_2$ and $O_2$. When the PEMFC cathode ($O_2$) and the anode ($H_2$) gases interact as an electrochemical process, the concentration of the $H_2$ and $O_2$ at the two electrodes will be consumed, that is lower than the initial concentration, and the irreversible loss caused by this concentration gradient is called the concentration over potential [31, 32]. The concentration over potential can be expressed as $V_{conc} = CLn(\frac{i_L}{i_L - i})$. Where $i_L$ indicates that the PEMFC can reach the limiting current density during operation and $c$ indicates the concentration loss constant [33].

**2.2. Modelling and simulation.**

The details mechanism of the PEM fuel cells are very complex due to the different and tightly phenomenon which occur within a cell-fluid-dynamic, migration, electrochemical reaction, diffusions, water transports inside polymer membrane involving both electro-osmotic drag and back diffusion, proton transports via proton-conductivities of the polymer membranes, electron conduction via electrically conductivities of the cell components, heat transfer involving both conduction via solids components of the cells and convection of reactant gases and cooling medium, water transports both evaporation and liquids via porous catalyst layer and gas diffusion layer , and phase changes (scheme 4 ). Modelling is needed for describing the basica phenomenon to evaluate the cells steady-state and dynamic behavior. However, the complex mechanism inside the fuel cell causes challenging in some models involving reactants, cooling, and humidification and conditioning systems. Models are able to predict fuel cell efficiency under different operating situations and optimization and designing of control systems [34-37].

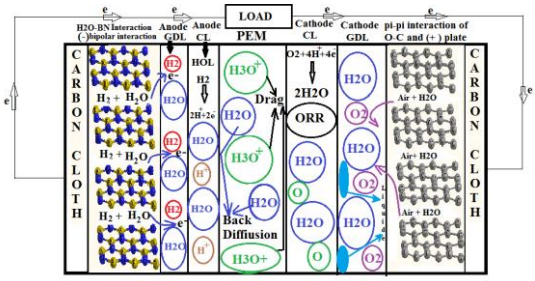


**Scheme 4.** Processing and operating of a PEM fuel cell.

In past decades, several of PEM fuel cell models are defined to the purpose of gas channel, gas diffusion layers, catalyst layers and polymer membrane of electrolyte [35, 36]. Models can also be categorized based on their dimension, single, double or triple which can be considered either isothermal or non-isothermal [37]. Single cell model explains the electrochemical and transporting processes in the fuel cell component including pressure drop, flow distribution, and temperature profile in the gas channel. This simulation, quantitatively explain interaction between physical and electrochemical phenomenon which can also be divided into two sections, first an empirical simulation for prediction how the fuel cell voltages change with the current densities with polarization curves[38] and second principle simulation is built-up from ordinary differential equations or solving partial differential equations ((PDEs) including distributed parameter, Stefan-Maxwell convection and diffusion account for species conservation. Based on Darcy's law, the principle of mass conservation is applied to simulate reactant concentration. Recently, in advance simulation, two-dimensional and three dimensional simulations have been developed. The two-dimensional simulation can be separated into two classes, first one explains the plane perpendicular to the flow channels and second describes the direction along the flow channel [39, 40]. An extended simulation of 3-dimensional, 2-phase, non-isothermal unit cell systems was investigated by Tao [38] for performing

parameters sensitivities examination. Generally, simulated systems are lumped data of parameters for evaluating fuel cell efficiency under various operating situations for any controlling as a function of time through solving differential equations (ODEs). Pukrushpan [37] investigated a system including fuel cell stack, hydrogen supply, air supply, cooling and the humidification systems with a constant temperature due to the dynamics variables.

**2.3. Inputs and outputs parameters for the simulation:**

Six input parameters are applied for any simulation involving voltage *U*, cooling temperature$T_{cool}$, hydrogen inlet $(n_{H_2^{in}}^{Anode})$, anode water inlet $(n_{H2O_{in}}^{Anode})$ Air inlet $(n_{Air_{in}}^{Cathode})$and the cathode water inlet $(n_{H2O_{in}}^{Cathode})$ while the output parameters are current "I" and temperature "T" and Gas channels (GCs) are the trajectory for flow of reactant gases. The common equation for mass conservation is as: $\frac{\partial \rho}{\partial T} + \nabla.(\rho\vartheta) = 0$ , **(5)** where $\nabla. = \frac{\partial}{\partial z} + \frac{\partial}{\partial y}$, $\rho$ and $\vartheta$ are density and velocity vector, respectively. The first term correspond to accumulation of mass as a function of time and the second term correspond with the mass flow changing [31]. Derived from equation (5), the mass balance for the anode and cathode gases channels are given by $\frac{\partial C_i^j}{\partial t} = -\frac{\partial \vartheta^j C_i^j}{\partial z} - \frac{n_i^j}{\delta^j}$ **(6)** where channel thickness in y-direction $\delta^j$ . In this kind modeling is better to apply the molar mass instead of mass; therefore the boundary equation is given by: $\vartheta^j C_i^j \,|\, 0, t = n_{i,n}^j$ which the superscript *j* is denoted both anode and cathode. On the anode side " *i* " , can be either $H_2$ or $H_2O$ and on the cathode it can be either O2, N2 or H2O and $n_i^j$ denote molar flow densities between gas channels and gas diffusion layers meanwhile $(n_{i,n}^j)$ denote inlet molar flow densities (positive in direction towards membrane for both sides). The general equation for mass conservation is given by: $\frac{dC_{i,k}^j}{dt} = -\frac{\vartheta_k^j C_{i,k}^j - \vartheta_{k-1}^j C_{i,k-1}^j}{\Delta z} - \frac{n_{i,k}^j}{\delta^j}$ **(7)** where *k* = 1, 2 , **…***n*-1, *n* The boundary condition is $\vartheta_0^j C_{i,0}^j \,|\, 0, t = n_{i,in}^j$ which is for the beginning of gas channel and $n_{i,in}^j$ is inlet molar flow densities. Usually, velocities vectors for flow can be estimated through Navier-Stokes equations without the acceleration terms and it can be simplified pressure drop relation (similar to Darcy's law) as follows: $\vartheta^j = -K^j \frac{\partial P^j}{\partial z}$ , Considering the boundary position at the outlet of the gas channels is equal to ambient pressure, therefore: $P^j(L_z, t) = P^{amb}$. Discretization of flow velocities for both anode and cathode gas channels is given by $\vartheta_k^j = -K^j \frac{P_{K+1}^j - P_k^j}{\Delta z}$ and by considering boundary situation $\vartheta_n^j = -K^j \frac{P^{amb} - P_n^j}{\Delta z}$. In addition in viewpoint of an ideal gas pressure in the gas can be calculated as: $P^j = RT^j \sum_i C_i^j$ and for a discretized equation $P_k^j = RT_k^j \sum_i C_{i,k}^j$ [41-45].

*2.3.1: Energy equilibrium and gas diffusion.* Storing energies in the channels systems is based on equation as follows $\frac{\partial(\rho\vartheta)^j}{\partial t} = -\frac{\partial}{\partial z}\left(\sum_i \vartheta^j C_i^j h_i T^j\right) + \lambda^j \left(\frac{\partial^2 T^j}{\partial z^2}\right) + \frac{\alpha_1}{\delta^j}(T - T^j) - \sum_i \frac{n_i^j}{\delta^j} h_i(T^j)$. Where the first term denotes energy transport in the z- orientation and the second and third terms are heat conduction and heat transfer, respectively. The forth term explains convective flow from gas channels or enthalpy transport. Through a thermodynamic equation of state temperature in the gas channels can be calculated as: $(\rho\vartheta) + p^j = \sum_i C_i^j h_i (T^j)$ . Gas diffusion layer appears among the catalyst layers and also the gas channels electrodes or collectors. The Stefan-Maxwell diffusion [32] for gas mixtures in *y*-orientation is given by $-\nabla\xi_i^j = \sum_{ks} \frac{\bar{\xi}_i^j n_i^j - \bar{\xi}_i^j n_{k,s}^j}{\bar{c}^j D_{i,ks}^{eff}}$ where $\xi_i^j$ is the mole fraction of gas species in the gas channels and $D_{i,ks}^{eff}$ is the gas diffusion coefficient between. Here "j "means cathode or anode section and if *j*=anode then i= H2, H2O and if *j*= cathode then *i* = O2, N2, H2O, in addition KS *is* also used for denoting gas species. In the *y*-orientation, the gradient of mole fractions " $\nabla\xi_i^j$" is given by $\nabla\xi_i^j = \frac{\xi_i^{cj} - \xi_i^j}{\delta^{Gj}}$ where$\xi_i^{cj}$ and $\delta^{Gj}$ are mole fractions in the catalyst and the thickness of gas diffusion, respectively meanwhile the molar fraction is given by $\bar{\xi}_i^j = 1/2(\xi_i^{cj} + \xi_i^j)$ [46-50]. Based on our previous works we have simulated the concepts of physical chemistry and computational methods for modeling the fuel cells to predict the high efficiency and mechanism of controlling [51-78].

## 3. RESULTS

Power density *P* of PEMFC in an irreversible path is depending on several variables including operating temperature *T*, working pressure *a*, proton exchange membrane water content λ or membrane water or membrane relative humidity ( $\emptyset_m$) parameter and the proton membrane thickness $d_{mem}$ and current density *i*, which can be expressed as $p = f(T, i, a, \lambda, d_{mem})$. It is important to keep some variables as a constant parameter such as working pressure *a*, the water content λ, and $d_{mem}$of, therefore the output power density is only a function of two variables *i* & *T* as *P= f (i, T*). In isotherm of *T*, the output power densities of the irreversible PEMFC is function of current density, *P = f* (*i*). When the operating temperature of the irreversible PEMFC is $T_1$, $T_2$, ….$T_n$ the maximum output power densities are $P_{max}(1)$, $P_{max}(2)$, $P_{max}(n)$, respectively of an irreversible PEMFC in a finite time. Alike with the effect of $a, \lambda, and\ d_{mem}$ on its optimal output power density can also be discussed as same the above equation [Fig.4].

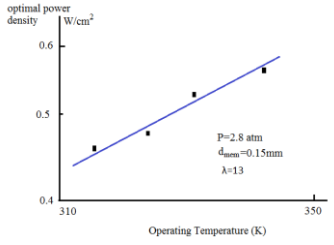


**Figure 4.** Optimal output power densities as a function of temperature.

It can be realized that the optimal output power densities of the irreversible PEMFC increase with the increasing of the operating temperature in the finite times. Obviously, due to the increase of *T*, the exchange current densities should be increased, the activation over potentials are reduced, and the proton pass rates have to be increased, as a result of the Ohmic over potentials and power dissipation are reduced. In small power dissipation, the minimum entropy production also decreases.

Consequently, increasing the operating temperature of the PEMFC can impressively develop its optimal output power densities in an appropriate working range. Increasing the operating pressure can also increase the density power of the irreversible PEMFC due to the increasing exchange current densities and decreasing activation over potential. Consequently the irreversibility of the irreversible PEMFC is diminished and the reversibility is elevated and the minimum entropies are decreased (fig.5).

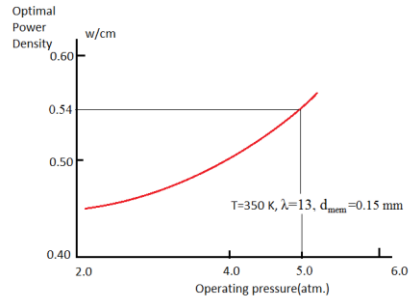


**Figure 5.** Optimal output power densities as a function of pressure.

As it can be seen corresponding optimal output power densities of pressures 3 and 4atm, are 0.46 and 0.505 W/cm$^2$, respectively. By increasing pressure from 3 atm. to 5 atm., the optimal output power densities are increased by 9.8% and also By increasing pressure from 4 atm. to 5 atm. the optimal output power densities are increased by 6.9% which means, the irreversible PEMFC can further improve its optimal output power density by suitably increasing its operating pressure during finite time operations.

Our calculation exhibits a maximum output power density through increasing the proton membrane thickness and this phenomenon is due to increase the hindrance of ions via the proton exchange membrane. Simultaneously, the Ohmic loss has been growth, the output power densities are decreased, and the maximum output power is also decreased (Fig. 6). With a proton exchange membrane thickness is around 0. 15 mm, the corresponding optimal output power density is 0.515 W/cm$^2$; when the proton exchange membrane thickness is 0. 20 mm, the corresponding optimal output power density is 0.415 W/cm$^2$.

This shows that when the proton membrane thickness is decreased from 0.020 cm to 0.015 cm, the optimal output power density is increased by 24%. As a result, reducing the thickness of the proton exchange membrane can increase the optimal output power density of the fuel cell in the finite times. It is notable that the thickness should not be thin less than a level, due to avoiding needle punching or cracking. Increasing the water content of the proton membrane can also promote the efficiency of the irreversible PEMFC, as result optimal output power density.

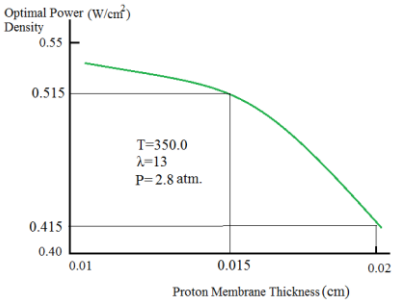


**Figure 6.** Optimal output power densities as a function of thickness.

Within the membrane water content of λ = 6, the optimal output power density is only 0.3 W/cm2, which indicates that the performance of PEMFC is seriously degraded when the water content of the membrane is too small; when the membrane water content λ = 20, that is, the water content of the proton membrane reaches saturation state, The optimal output power density is only 0.48 W/cm2. The optimal output power density of the PEMFC increased by 15.6% when the water content of the proton exchange membrane increased from λ = 1 λ = 20(Fig.7).

Controlling the water contents of the protons exchange membranes between the ideal state and the saturated state at any time can strongly improve the optimal output power densities of an irreversible PEMFC [79-86].

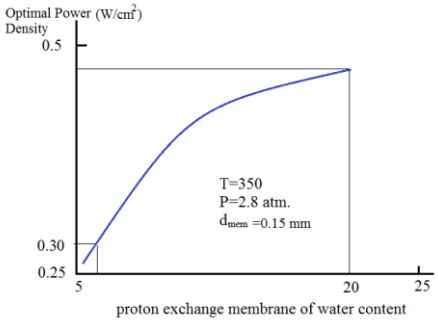


**Figure 7**. Proton exchange membrane of water in 350K and 2.8 atm.

## 4. CONCLUSIONS

Hydrogen fuel cells will play a significant role in the transportation industry in the near future. The price of fuel cells will reduce in producing fuel cells in large quantities and commercializing them. Modelling and controlling of ion transport rate efficiency can be investigated for various fuel cells in viewpoint of voltage output data. Effects of operating data including temperature (T), pressure (P), proton exchange membrane water content (λ), and proton exchange membrane thickness ($d_{mem}$) on the optimal performance of the irreversible fuel cells have been studied. Performance of fuel cells was analyzed by simulating polarization and power curves for a fuel cell operating at various conditions with current densities. Controlling T, P, $d_{mem}$ , and the water contents (λ) of the proton exchange membranes between the ideal state and the saturated state at any time can strongly improve the optimal output power densities of an irreversible PEMFC , AFC, DMFC, PAFC, DFAFC, and DCFC fuel cells.

## 5. REFERENCES

1. Schmidt-Rohr, K. Batteries Store and Release Energy: Explaining Basic Electrochemistry. *J. Chem. Educ*. **2018** *95*, 1801-1810, https://doi.org/10.1021/acs.jchemed.8b00479.

2. Ciureanu, M. Effects of nafion dehydration in pem fuel cells. *Journal of Applied Electrochemistry* **2004**, *34*, 705-714, https://doi.org/10.1023/B:JACH.0000031102.32521.c6.

3. Cruz-Manzo, S.; Chen, R.; Rama, P. Study of current distribution and oxygen diffusion in the fuel cell cathode catalyst

layer through electrochemical impedance spectroscopy. *International Journal of Hydrogen Energy* **2013**, *38*,1702- 1713, https://doi.org/10.1016/j.ijhydene.2012.08.141.

4. de Bruijn, F.A.; Dam, V.A.T.; Janssen GJM. Review: Durability and degradation issues of PEM fuel cell components. *Fuel Cells*, **2008**, *8*, 22, https://doi.org/10.1002/fuce.200700053

5. Wang, J.Y. Pressure drop and flow distribution in parallel-channel of configurations of fuel cell stacks: U-type arrangement". *International Journal of Hydrogen Energy* **2008**, *33*, 6339–6350, https://doi.org/10.1016/j.ijhydene.2008.08.020.

6. Dohle, H.; Mergel, J.; Stolten, D. Heat and power management of a direct-methanol-fuel-cell (DMFC) system. *Journal of Power Sources* **2002**, *111*, 268-282, https://doi.org/10.1016/S0378-7753(02)00339-7.

7. Wei, Y.; Matar, S.; Shen, L.; Zhang, X.; Guo, Z.; Zhu, H.; Liu, H. A novel membrane for DMFC – Na2Ti3O7 Nanotubes/Nafion @ composite membrane: Performances studies. *International Journal of Hydrogen Energy* **2012**, *37*, 1857–1864, https://doi.org/10.1016/j.ijhydene.2011.08.107.

8. Saif, M.; Liu, H. Effect of cathode catalyst layer thickness on methanol cross-over in a DMFC. *Electrochimica Acta* **2010**, *56*, 600 – 606, https://doi.org/10.1016/j.electacta.2010.09.001.

9. Saif, A.; Liu, H, Separate measurement of current density under land and channel in Direct Methanol Fuel Cells. *Journal of Power Sources* **2014**, *246*, 899–905, https://doi.org/10.1016/j.jpowsour.2013.08.029.

10. Motoo, S.; Watanabe, M. Electrolysis by Ad-Atoms Part II. Enhancement of the Oxidation of Methanol on Platinum by Ruthenium Ad-Atoms. *Electrochemistry and Interfacial Electrochemistry* **1975**, *60*, 267–273, http://dx.doi.org/10.1016/S0022-0728(75)80261-0.

11. Ha, S.; Larsen, R.; Masel, R.I. Performance characterization of Pd /C Nano-catalyst for direct formic acid fuel cells. *Journal of Power Sources* **2005**, *144*, 28–34, https://doi.org/10.1016/j.jpowsour.2004.12.031.

12. Litster, S.; McLean, G. PEM fuel cell electrodes. *Journal of Power Sources* **2004**, *130*, 61-76, https://doi.org/10.1016/j.jpowsour.2003.12.055.

13. Schmittinger, W.; Vahidi, A. A review of the main parameters influencing long term performance and durability of PEM fuel cells. *Journal of Power Sources* **2008**, *180*, 1-14, https://doi.org/10.1016/j.jpowsour.2008.01.070.

14. Borup, R. Scientific aspects of polymer electrolyte fuel cell durability and degradation. *Chemical reviews* **2007**, *107*, 3904-3951, https://doi.org/10.1021/cr050182l.

15. Su, A.; Weng, F.; Hsu, C.; Chen, Y. Studies on flooding in PEM fuel cell cathode channels. *International Journal of Hydrogen Energy* **2006**, *31*, 1031-1039, https://doi.org/10.1016/j.ijhydene.2005.12.019.

16. Pasaogullari, U.; Wang, C. Two-phase modeling and flooding prediction of polymer electrolyte fuel cells. *Journal of the Electrochemical Society* **2005**, *152*, 380-390, http://dx.doi.org/10.1149/1.1850339.

17. Futerko, P.; Hsing, I. Two-dimensional finite-element method study of the resistance of membranes in polymer electrolyte fuel cells. *Electrochimica Acta* **2000**, *45*,1741-1751, https://doi.org/10.1016/S0013-4686(99)00394-1.

18. Dutta, S.; Shimpalee, S.; Van Zee, J.W. Three-dimensional numerical simulation of straight channel pem fuel cells. *Journal of Applied Electrochemistry* **2000**, *30*, 135-146, https://doi.org/10.1023/A:1003964201327.

19. Wang, Z.H.; Wang, C.Y.; Chen, K.S. Two-phase flow and transport in the air cathode of proton exchange membrane fuel cells. *Journal of Power Sources* **2001**, *94*, 40-50, https://doi.org/10.1016/S0378-7753(00)00662-5.

20. He, W.; Lin, G.; Van Nguyen, T. Diagnostic tool to detect electrode flooding in proton-exchange-membrane fuel cells. *AIChE Journal* **2003**, *49*, 3221-3228, https://doi.org/10.1002/aic.690491221.

21. Bosco, A D.P.; Fronk, M.H. Fuel cell flooding detection and correction. *US Patent* **2000**, *6*,103,409.

22. Mollaamin, F.; Monajjemi, M. Harmonic linear combination and normal mode analysis of semiconductor nanotubes vibrations, *journal of Computational and Theoretical Nanoscience*, **2015**, *12(6)*, 1030-9

23. Dutta, S.; Shimpalee, S.; Van Zee, J.W. Numerical prediction of mass-exchange between cathode and Anode Channels in a PEM Fuel Cell. *Int. J. Heat Mass Transfer* **2001**, *44*, 2029-2042, http://dx.doi.org/10.1016/S0017-9310(00)00257-

24. Cussler, E.L. *Diffusion Mass Transfer in Fluid Systems*, Cambridge University. Press, Cambridge, 1997, pp. 101, https://doi.org/10.1017/CBO9780511805134.

25. Lum, K.W. *Three Dimensional Computational Modelling of a Polymer Electrolyte Fuel* University of Loughborough, **2003**.

26. Yuan, D.Q. The analytical method of finite time thermo dynamics about the physical and the chemical performances of the fuel cell. *Chin. J. Chem. Phys.* **1999**, *12*, 63–66.

27. Yan, Z.J. Comment on: The analytical method of finite time thermodynamics about the physical and the chemical performances of the fuel cell. *Chin. J. Chem. Phys.* **2001**, *14*, 378–380.

28. Yuan, D.Q. Reply to Comment on: The analytical method of finite time thermodynamics about the physical and the chemical performances of the fuel cell. *Chin. J. Chem. Phys.* **2001**, *14*, 381–383.

29. Yin, S.L. Ecological Optimization for a Hybrid System Integrating a Phosphoric Acid Fuel Cell with an Absorption Refrigerator. Master's Thesis. Donghua University, Shanghai China, 2017.

30. Wei, F.F. The Optimal Thermodynamic Research and Application of Proton Exchange Membrane Fuel Cells. Master's Thesis, Donghua University, Shanghai, China, 2013.

31. Chen, X.; Li, W.B.; Gong, G.C. Parametric analysis and optimization of PEMFC system for maximum power and efficiency using MOEA/D. *Appl. Therm. Eng.* **2017**, *121*, 400–409, https://doi.org/10.1016/j.applthermaleng.2017.03.144.

32. Li, C.J.; Liu, Y.; Ma, Z.S. Thermodynamic analysis of the performance of an irreversible PEMFC. *Defect Diffuse.Forum* **2018**, *388*, 350–360, https://doi.org/10.4028/www.scientific.net/DDF.388.350.

33. Barbir, F.; Gorgun, H.; Wang, X. Relationship between pressure drop and cell resistance as a diagnostic tool for PEM fuel cells. *J. Power Sources* **2017**, *141*, 96–101, https://doi.org/10.1016/j.jpowsour.2004.08.055.

34. Rowe, A.; Li, X. Mathematical modeling of proton exchange membrane fuel cells. *Journal of Power Sources* **2001**, *102*, 82-96, https://doi.org/10.1016/S0378-7753(01)00798-4.

35. Siegel, C. Review of computational heat and mass transfer modeling in polymer electrolyte-membrane (pem) fuel cells. *Energy* **2008**, *33*, 1331-1352, https://doi.org/10.1016/j.energy.2008.04.015.

36. Yao, K.Z.; Karan, K.; McAuley, K.B.; Oosthuizen, P.; Peppley, B.; Xie, T. A review of mathematical models for hydrogen and direct methanol polymer electrolyte membrane

fuel cells. *Fuel Cells* **2004**, *4*, 3-29, https://doi.org/10.1002/fuce.200300004.
37. Pukrushpan, J.T.; Peng, H.; Stefanopoulou, A.G. Control-oriented modeling and analysis for automotive fuel cell systems. *Journal of Dynamic Systems, Measurement, and Control* **2004**, *126*, 14, https://doi.org/10.1016/S1474-6670(17)30386-5.
38. Tao, W.Q.; Min, C.H.; Liu, X.L.; He, L.Y.; Yin, B.H.; Jiang, W. Parameter sensitivity examination and discussion of PEM fuel cell simulation model validation: Part i. current status of modeling research and model development. *Journal of Power Sources* **2006**, *160*, 359-373, https://doi.org/10.1016/j.jpowsour.2006.01.078.
39. Karimi, G. Along-channel flooding prediction of polymer electrolyte membrane fuel cells. *International Journal of Energy Research* **2011**, *35*, 883-896, https://doi.org/10.1002/er.1746 .
40. Eriksson, E.L.V.; Gray, E.M.A. Optimization and integration of hybrid renewable energy hydrogen fuel cell energy systems—A critical review. *Appl. Energy* **2017**, *202*, 348–364, https://doi.org/10.1016/j.apenergy.2017.03.132.
41. Costilla-Reyes, A.; Erbay, C.; Carreon-Bautista, S.; Han, A.; Sánchez-Sinencio, E. A Time-Interleave-Based Power Management System with Maximum Power Extraction and Health Protection Algorithm for Multiple Microbial Fuel Cells for Internet of Things Smart Nodes. *Appl. Sci.* **2018**, *8*, 2404, https://doi.org/10.3390/app8122404.
42. Kerviel, A.; Pesyridis, A.; Mohammed, A.; Chalet, D.; Kerviel, A.; Pesyridis, A.; Mohammed, A.; Chalet, D. An Evaluation of Turbocharging and Supercharging Options for High-Efficiency Fuel Cell Electric Vehicles. *Appl. Sci.* **2018**, *8*, 2474, https://doi.org/10.3390/app8122474.
43. Somekawa, T.; Nakamura, K.; Kushi, T.; Kume, T.; Fujita, K.; Yakabe, H. Examination of a high-efficiency solid oxide fuel cell system that reuses exhaust gas. *Appl. Therm. Eng.* **2017**, *114*, 1387–1392, https://doi.org/10.1016/j.applthermaleng.2016.10.096.
44. Chakraborty, U.K. A New Model for Constant Fuel Utilization and Constant Fuel Flow in Fuel Cells. *Appl. Sci.* **2019**, *9*, 1066, https://doi.org/10.3390/app9061066.
45. Choi, H.; Shin, J.; Woo, J. Effect of electricity generation mix on battery electric vehicle adoption and its environmental impact. *Energy Policy* **2018**, *121*, 13–24, https://doi.org/10.1016/j.enpol.2018.06.013.
46. Boretti, A. Novel dual fuel diesel-ammonia combustion system in advanced TDI engines. *Int. J. Hydrogen Energy* **2017**, *42*, 7071–7076, https://doi.org/10.1016/j.ijhydene.2016.11.208.
47. Hibino, T.; Kobayashi, K.; Nagao, M.; Teranishi, S. Hydrogen Production by Direct Lignin Electrolysis at Intermediate Temperatures. *ChemElectroChem* **2017**, *4*, 3032–3036, https://doi.org/10.1002/celc.201700917.
48. Hori, T.; Ma, Q.; Kobayashi, K.; Nagao, M. Electrolysis of humidified methane to hydrogen and carbon dioxide at low temperatures and voltages. *Int. J. Hydrogen Energy* **2019**, *44*, 2454–2460, https://doi.org/10.1016/j.ijhydene.2018.12.044.
49. Yang, G.; Jung, W.; Ahn, S.J.; Lee, D.; Yang, G.; Jung, W.; Ahn, S.-J.; Lee, D. Controlling the Oxygen Electrocatalysis on Perovskite and Layered Oxide Thin Films for Solid Oxide Fuel Cell Cathodes. *Appl. Sci.***2019**, *9*, 1030, https://doi.org/10.3390/app9051030
50. Wilberforce, T.; El-Hassan, Z.; Khatib, F.N.; Al Makky, A.; Baroutaji, A.; Carton, J.G.; Olabi, A.G. Developments of electric cars and fuel cell hydrogen electric cars. *Int. J. Hydrogen Energy* **2017**, *42*, 25695–25734, https://doi.org/10.1016/j.ijhydene.2017.07.054
51. Mollaamin, F. Monajjemi, M. DFT outlook of solvent effect on function of nano bioorganic drugs. *Physics and Chemistry of Liquids* **2012**, *50*, 596-604, https://doi.org/10.1080/00319104.2011.646444.
52. Mollaamin, F.; Gharibe, S.; Monajjemi, M. Synthesis of various nano and micro ZnSe morphologies by using hydrothermal method. *International Journal of Physical Sciences* **2011**, *6*, 1496-1500.
53. Ardalan, T.; Ardalan, P.; Monajjemi, M. Nano theoretical study of a C 16 cluster as a novel material for vitamin C carrier. *Fullerenes Nanotubes and Carbon Nanostructures* **2014,** *22*, 687-708, https://doi.org/10.1080/1536383X.2012.717561.
54. Mahdavian, L.; Monajjemi, M.; Mangkorntong, N. Sensor response to alcohol and chemical mechanism of carbon nanotube gas sensors. *Fullerenes Nanotubes and Carbon Nanostructures* **2009,** *17*, 484-495, https://doi.org/10.1080/15363830903130044.
55. Monajjemi, M.; Najafpour, J. Charge density discrepancy between NBO and QTAIM in single-wall armchair carbon nanotubes. *Fullerenes Nanotubes and Carbon Nano structures* **2014**, *22*, 575-594, https://doi.org/10.1080/1536383X.2012.702161.
56. Monajjemi, M.; Hosseini, M.S. Non bonded interaction of B16 N16 nano ring with copper cations in point of crystal fields. *Journal of Computational and Theoretical Nanoscience* **2013**, *10*, 2473- 2477.
57. Monajjemi, M.; Mahdavian, L.; Mollaamin, F. Characterization of nanocrystalline silicon germanium film and nanotube in adsorption gas by Monte Carlo and Langevin dynamic simulation. *Bulletin of the Chemical Society of Ethiopia* **2008**, *22*, 277-286, http://dx.doi.org/10.4314/bcse.v22i2.61299.
58. Lee, V.S.; Nimmanpipug, P.; Mollaamin, F.; Thanasanvorakun, S.; Monajjemi, M. Investigation of single wall carbon nanotubes electrical properties and normal mode analysis: Dielectric effects. *Russian Journal of Physical Chemistry A* **2009**, *83*, 2288-2296, https://doi.org/10.1134/S0036024409130184.
59. Mollaamin, F.; Najafpour, J.; Ghadami, S.; Akrami, M.S.; Monajjemi, M. The electromagnetic feature of B N H (x = 0, 4, 8, 12, 16, and 20) nano rings:Quantum theory of atoms in molecules/NMR approach. *Journal of Computational and Theoretical Nanoscience* **2014**, *11*, 1290-1298.
60. Monajjemi, M.; Mahdavian, L.; Mollaamin, F.; Honarparvar, B. Thermodynamic investigation of enolketo tautomerism for alcohol sensors based on carbon nanotubes as chemical sensors. *Fullerenes Nanotubes and Carbon Nanostructures* **2010**, *18*, 45-55, https://doi.org/10.1080/15363830903291564.
61. Monajjemi, M.; Ghiasi, R.; Seyed Sadjadi, M.A. Metal-stabilized rare tautomers: N4 metalated cytosine (M = Li , Na , K , Rb and Cs ), theoretical views. *Applied Organometallic Chemistry* **2003**, *17*, 635-640, https://doi.org/10.1002/aoc.469.
62. Ilkhani, A.R.; Monajjemi, M. The pseudo Jahn-Teller effect of puckering in pentatomic unsaturated rings C AE , A=N, P, As, E= H, F, Cl.*Computational and Theoretical Chemistry* **2015**, *1074*, 19-25.
63. Monajjemi, M. Non-covalent attraction of B N and repulsion of B N in the B N ring: a quantum rotatory due to an external field. *Theoretical Chemistry Accounts* **2015**, *134*, 1-22, https://doi.org/10.1007/s00214-015-1668-9.
64. Monajjemi, M.; Naderi, F.;Mollaamin, F.; Khaleghian, M. Drug design outlook by calculation of second virial coefficient as a nano study. *Journal of the Mexican Chemical Society* **2012**, *56*, 207-211.

65. Monajjemi, M.; Bagheri, S.; Moosavi, M.S. Symmetry breaking of B2N(-,0,+): An aspect of the electric potential and atomic charges. *Molecules* **2015,** *20*, 21636-21657, https://doi.org/10.3390/molecules201219769.
66. Monajjemi, M.; Mohammadian, N.T. S-NICS: An aromaticity criterion for nano molecules. *Journal of Computational and Theoretical Nanoscience* **2015**, *12*, 4895-4914, https://doi.org/10.1166/jctn.2015.4458.
67. Monajjemi, M.; Ketabi, S.; Hashemian Zadeh, M.; Amiri, A. Simulation of DNA bases in water: Comparison of the Monte Carlo algorithm with molecular mechanics force fields. *Biochemistry (Moscow)* **2006**, *71*, 1-8.
68. Monajjemi, M.; Lee, V.S.; Khaleghian, M.; Honarparvar, B.; Mollaamin, F. Theoretical Description of Electromagnetic Nonbonded Interactions of Radical, Cationic, and Anionic NH2BHNBHNH2 Inside of the B18N18 Nanoring. *J. Phys. Chem C* **2010**, *114*, 15315, http://dx.doi.org/10.1021/jp104274z.
69. Monajjemi, M.; Boggs, J.E. A New Generation of BnNn Rings as a Supplement to Boron Nitride Tubes and Cages. *J. Phys. Chem. A* **2013**, *117*, 1670-1684, http://dx.doi.org/10.1021/jp312073q.
70. Monajjemi, M. Non bonded interaction between BnNn (stator) and BN B (rotor) systems: A quantum rotation in IR region. *Chemical Physics* **2013**, *425*, 29-45, https://doi.org/10.1016/j.chemphys.2013.07.014.
71. Monajjemi, M.; Robert, W.J.; Boggs, J.E. NMR contour maps as a new parameter of carboxyl's OH groups in amino acids recognition: A reason of tRNA–amino acid conjugation. *Chemical Physics* **2014**, *433*, 1-11, https://doi.org/10.1016/j.chemphys.2014.01.017.
72. Monajjemi, M. Quantum investigation of non-bonded interaction between the B15N15 ring and BH2NBH2 (radical, cation, and anion) systems: a nano molecularmotor. *Struct Chem* **2012,** *23*, 551–580, http://dx.doi.org/10.1007/s11224-011-9895
73. Monajjemi, M. Metal-doped graphene layers composed with boron nitride–graphene as an insulator: a nano-capacitor. *Journal of Molecular Modeling* **2014**, *20*, 2507, https://doi.org/10.1007/s00894-014-2507-y.
74. Monajjemi M. Graphene/(h-BN)*n*/X-doped raphene as anode material in lithium ion batteries (X = Li, Be, B AND N). *Macedonian Journal of Chemistry and Chemical Engineering* **2017**, *36*, 101–118, http://dx.doi.org/10.20450/mjcce.2017.1134.
75. Monajjemi, M. Cell membrane causes the lipid bilayers to behave as variable capacitors: A resonance with self-induction of helical proteins. *Biophysical Chemistry* **2015**, *207*, 114-127, https://doi.org/10.1016/j.bpc.2015.10.003.
76. Monajjemi, M. Study of CD5+ Ions and Deuterated Variants (CHxD(5-x)+): An Artefactual Rotation. *Russian Journal of Physical Chemistry a* **2018,** *92*, 2215-2226.
77. Monajjemi, M. Liquid-phase exfoliation (LPE) of graphite towards graphene: An ab initio study. *Journal of Molecular Liquids* **2017**, *230*, 461–472.
78. Jalilian, H.; Monajjemi, M. Capacitor simulation including of X-doped graphene (X = Li, Be, B) as two electrodes and (h-BN)m (m = 1–4) as the insulator. *Japanese Journal of Applied Physics* **2015**, 54, 085101-7.
79. Bhosale, A.C.; Mane, S.R.; Singdeo, D.; Ghosh, P.C. Modeling and experimental validation of a unitized regenerative fuel cell in electrolysis mode of operation. *Energy* **2017**, *121*, 256–263. https://doi.org/10.1016/j.energy.2017.01.031
80. Ito, H.; Miyazaki, N.; Ishida, M.; Nakano, A. Efficiency of unitized reversible fuel cell systems. *Int. J. Hydrogen Energy* **2016**, *41*, 5803–5815.
81. Hardman, S.; Tal, G. Who are the early adopters of fuel cell vehicles? *Int. J. Hydrogen Energy* **2018**, *43*, 17857–17866, https://doi.org/10.1016/j.ijhydene.2018.08.006.
82. Robledo, C.B.; Oldenbroek, V.; Abbruzzese, F.; van Wijk, A.J.M. Integrating a hydrogen fuel cell electric vehicle with vehicle-to-grid technology, photovoltaic power and a residential building. *Appl. Energy* **2018**, *215*, 615–629, https://doi.org/10.1016/j.apenergy.2018.02.038.
83. Brey, J.J.; Carazo, A.F.; Brey, R. Exploring the marketability of fuel cell electric vehicles in terms of infrastructure and hydrogen costs in Spain. *Renew. Sustain. Energy Rev.* **2018**, *82*, 2893–2899, https://doi.org/10.1016/j.rser.2017.10.042.
84. He, X.; Jiang, Y. Review of hybrid electric systems for construction machinery. *Autom. Constr.* **2018**, *92*, 286–296, https://doi.org/10.1016/j.autcon.2018.04.005.
85. Dreier, D.; Silveira, S.; Khatiwada, D.; Fonseca, K.V.O.; Nieweglowski, R.; Schepanski, R. Well-to-Wheel analysis of fossil energy use and greenhouse gas emissions for conventional, hybrid-electric and plug-in hybrid-electric city buses in the BRT system in Curitiba, Brazil. *Transp. Res. Part D Transp. Environ.* **2018**, *58*, 122–138, https://doi.org/10.1016/j.trd.2017.10.015.
86. Bizon, N.; Thounthong, P. Fuel economy using the global optimization of the Fuel Cell Hybrid Power Systems. *Energy Convers. Manag.* **2018**, *173*, 665–678, https://doi.org/10.1016/j.enconman.2018.08.015.

## 6. ACKNOWLEDGEMENTS

This research is funded by Vietnam National University – Ho Chi Minh City (VNU-HCM) under the grant number TX2019-32-01